New lattice Boltzmann model for the compressible Navier-Stokes equations

Kataoka, Takeshi

Hanada, Takaya

(Citation)
International Journal for Numerical Methods in Fluids,91(4):183-197

(Issue Date)
2019-10-10

(Resource Type)
journal article

(Version)
Accepted Manuscript

New lattice Boltzmann model for the compressible Navier-Stokes equations

Takeshi Kataoka* and Takaya Hanada

Corresponding author: Takeshi Kataoka
Graduate School of Engineering, Kobe University,
Rokkodai, Nada, Kobe 657-8501, Japan

Tel: +81. 78. 803. 6143, Fax: +81. 78. 803. 6143

E-mail: kataoka@mech.kobe-u.ac.jp

SUMMARY

We have developed a fundamentally new type of simple lattice Boltzmann (LB) model for the compressible Navier-Stokes equations based on the kinetic system proposed by Sone. The model uses the kinetic equation of free-molecular type in the streaming process, and modifies the distribution function to its Chapman-Enskog type at each time step. Compared with the current LB models, the proposed model is superior in the following two points: (I) there are no inherent errors associated with the Knudsen number; (II) any flow parameters, including three transport coefficients, can be chosen freely according to our convenience. Numerical tests and error estimates confirm the above statements.

KEY WORDS: lattice Boltzmann method; compressible NS equations; compressible flows

1. INTRODUCTION

The lattice Boltzmann method (LBM) [1-4] is one of well-known numerical methods to obtain solutions of the fluid-dynamic-type equations. The LBM solves the kinetic equation with a finite number of molecular velocities such that the macroscopic variables obtained from the solution satisfy the desired fluid-dynamic-type equations. The merits of the LBM are the simple basic equation, the linear derivative terms, high resolution for capturing discontinuities like shock waves and high capability for detecting small oscillations like sound waves involved in fluid flows. Owing to these merits and various proposed models assessed by a quite significant number of researchers, the LBM has already grown into a well-established numerical tool for simulating compressible flows with shocks and contact discontinuities or aerodynamic sound. These LB models are also available even in commercial softwares like PowerFlow and X-flow.

The history of such fast development for compressible LBM started from the multi-speed (MS) model [1-4], which is a straightforward extension of the ordinary LBM. Many researchers have attempted to improve the LB models since then, especially to resolve the issues of limitation for choice of parameters (like the specific-heat ratio and Prandtl number) and numerical stability to high-speed-flow simulations. To address the first issue on adjustability of specific-heat ratio, some researchers introduced an extra energy into the definition of total internal energy [5-9]. He *et al*. [10] and Li et al. [11] took different approach to utilize two kinds of density distribution functions for the density and the additional internal energy to recover adjustability for both the specific-heat ratio and Prandtl number. This is called the double-distribution-function (DDF) model. In an effort to resolve the second issue, Qu *et al.* [12] replaced the conventional Maxwellian distribution function by a circular function and achieved satisfactory simulation results in high Mach number flows. Such low-Mach number constraint was also addressed by several techniques, such as the entropic method [13,14], the fix-up scheme [13,15], and dissipation [16-18]. Recently, Xu's group also made considerable contribution to improvement of LB models for high-speed compressible flows [19-22].

Despite such brilliant achievements and the state-of-the-art of LBM being already well developed and mature, there still remain several fundamental issues that should be resolved:

(i) Errors inherent to the Knudsen number appear.

(ii) Not all the flow parameters can be chosen freely. For instance, three transport coefficients, i.e. the viscosity, the bulk viscosity, and the thermal conductivity, cannot be chosen freely.

The first issue (i) means that when the Knudsen number is not small, which is often the case for the small Reynolds number flows, the LBM includes some inherent error. The second issue (ii) indicates

that current LBM cannot obtain some solutions. In order to address these issues, the ordinary method is to introduce some modifications, but such revisions in general lead to complicated scheme, and hence, prevent the LBM from being accepted by CFD users as a much more widely used solver for simulating flows. Therefore it is desired, after several decades of rapid LBM development, not to seek various modifications of existing models but to provide a fundamentally different new model that is free of any inherent issues mentioned above.

Sone [23] proposed a simple way to construct a kinetic system of equation in such a way that some moments of the solution of the kinetic system satisfy the desired equations (not only the Euler or NS equations but also the other equations) exactly. On the basis of this system, he discussed a much simpler numerical scheme which uses the free-molecular kinetic equation, but instead modifies the velocity distribution function at each time step to Chapman-Enskog type (see also Pullin [24] and Chou & Baganoff [25]). The error estimate of this scheme was also explained, and it was mentioned that the molecular velocity can be chosen to be discrete. This scheme overcomes the above-mentioned issues (i) and (ii).

In terms of computational efficiency, the LBM, although it is already well-established, still has two issues. First, there is a difficulty of computation of the BKW equation for small Knudsen numbers or small space lattice due to cancelation of many digits in the collision term (as noted in Sone [23]). To remedy this issue, some researchers resorted to multiple-relaxation-time (MRT) models and succeeded in overcoming this difficulty [20,21]. However, the MRT model is a bit complicated due to complexity of transformation matrix. The free-molecular equation to be presented in this paper is simple with no transformation matrix and no difficulty involved for small Knudsen number flows. The second issue is that additional computer memory is necessary in the computation of LBM because not only macroscopic variables but also the velocity distribution function must be memorized. In the kinetic system proposed by Sone, however, macroscopic variables can be calculated without velocity distribution function so that there is no need to store the velocity distribution function. In fact, Junk & Rao [26] (see also Inamuro [27]) devised such a model for incompressible flows, but there is no model for compressible flows.

In the present study therefore we develop a new type of lattice Boltzmann (LB) model that resolves the above issues. To this end, we will make the system by Sone [23] effective as a numerical solver by introducing discrete molecular velocities and the corresponding Chapman-Enskog-type velocity distribution function explicitly. The number and position of molecular velocities are dependent on the fluid-dynamic-type equations we want to solve, which are the compressible NS equations here. They are looked for under the constraint that some moments of the velocity distribution function satisfy the prescribed relations (see (24) below). The proposed model overcomes the above issues. Moreover this

model is very ‘simple’.

The present paper is arranged in the following order. In Section 2 the kinetic system proposed by Sone is briefly explained, and in Section 3 new LB model for the compressible NS equations is presented. Validity of the proposed model is tested in Section 4 for various flow cases including practical ones. In the last section (Section 5), concluding remarks follow.

2. KINETIC SYSTEM DEVELOPED BY SONE

In this section, we will briefly explain the kinetic system developed by Sone [23]. In Section 2.1, the method for constructing a kinetic equation replacing the general fluid-dynamic-type equations exactly is explained. On the basis of this method, in Section 2.2, we discuss a simple numerical system which employs the free-molecular kinetic equation in order to lay foundation for introducing new LB model in Section 3. For more details, see Appendix C in Sone [23].

2.1. Exact kinetic-equation system

Let x_α, c_α, η, and t ($\alpha = 1,2,\cdots,D$; D is the number of dimensions) be independent variables, and $f(x_\alpha, c_\alpha, \eta, t)$ be a dependent variable (or the velocity distribution function). Using the notation

$$\langle f \rangle = \int_{-\infty}^{\infty} \cdots \int_{-\infty}^{\infty} f \, dc_1 dc_2 \cdots dc_D d\eta \,, \tag{1}$$

the macroscopic variables ρ_r ($r = 0,1,\cdots,D+1$) are defined as

$$\rho_r = \langle \phi_r f \rangle, \tag{2}$$

where $\phi_r(c_\alpha, \eta)$ ($r = 0,1,\cdots,D+1$) are functions of c_α and η chosen appropriately depending on the specific situation. The flux H_α^r of the macroscopic variables is defined as

$$H_\alpha^r = \langle \phi_r c_\alpha f \rangle \,. \tag{3}$$

Taking a velocity distribution function f^{c} of the form

$$f = f^{\mathrm{c}}(\rho_r, \nabla\rho_r, c_\alpha, \eta) \,, \tag{4}$$

where the variables x_α and t enter only through the macroscopic variables ρ_r or their derivatives $\nabla\rho_r$ with ∇ being the representative of a collection of the derivatives $\partial^s / \partial x_{\alpha_1} \cdots \partial x_{\alpha_s}$ (this type of function f^{c} is called a function of Chapman-Enskog type), their moments are

$$\rho_r = \left\langle \phi_r f^{\mathrm{c}} \right\rangle, \quad H_\alpha^{r\,\mathrm{c}}(\rho_r, \nabla\rho_r) = \left\langle \phi_r c_\alpha f^{\mathrm{c}} \right\rangle. \tag{5a,b}$$

Using this function f^{c}, Sone[1] introduced the following initial-value problem of the kinetic equation:

$$\begin{aligned} \frac{\partial f}{\partial t} + c_\alpha \frac{\partial f}{\partial x_\alpha} &= c_\alpha \left(\frac{\partial f^{\mathrm{c}}}{\partial \rho_r} \frac{\partial \rho_r}{\partial x_\alpha} + \frac{\partial f^{\mathrm{c}}}{\partial \nabla\rho_r} \frac{\partial \nabla\rho_r}{\partial x_\alpha} \right) \\ &\quad - \left(\frac{\partial f^{\mathrm{c}}}{\partial \rho_r} + \frac{\partial f^{\mathrm{c}}}{\partial \nabla\rho_r} \nabla \right) \left(\frac{\partial H_\alpha^{r\,\mathrm{c}}}{\partial \rho_s} \frac{\partial \rho_s}{\partial x_\alpha} + \frac{\partial H_\alpha^{r\,\mathrm{c}}}{\partial \nabla\rho_s} \frac{\partial \nabla\rho_s}{\partial x_\alpha} \right), \end{aligned} \tag{6}$$

with the initial condition:

$$f = f^{\mathrm{c}}(\rho_r^{(0)}, \nabla\rho_r^{(0)}, c_\alpha, \eta) \quad \text{at} \quad t = t_0, \tag{7}$$

where the summation convention is applied to the subscripts α, r, and s. He then proved that the macroscopic variables ρ_r calculated from the solution f of the above set (6) and (7) are exact solution of the initial-value problem of the following partial differential equations:

$$\frac{\partial \rho_r}{\partial t} + \frac{\partial H_\alpha^{r\,\mathrm{c}}}{\partial x_\alpha} = 0, \tag{8}$$

with the initial condition:

$$\rho_r = \rho_r^{(0)} \quad \text{at} \quad t = t_0. \tag{9}$$

2.2. Simple numerical system

Let us consider to solve, instead of the complicated equation (6), the following simple free-molecular kinetic equation

$$\frac{\partial f}{\partial t} + c_\alpha \frac{\partial f}{\partial x_\alpha} = 0, \tag{10}$$

in a continuous sequence of time intervals $(t_0, t_1]$, $(t_1, t_2], \cdots$ under the initial condition for each interval $(t_m, t_{m+1}]$ given by

$$f = f^{\mathrm{c}}(\rho_r^{(m)}, \nabla\rho_r^{(m)}, c_\alpha, \eta) \quad \text{at} \quad t = t_m, \tag{11}$$

where $\rho_r^{(0)}$ are the real initial values at $t = t_0$, and $\rho_r^{(m)}$ ($m \neq 0$) are ρ_r calculated from the solution f at $t = t_m$ of (10) in the preceding interval $(t_{m-1}, t_m]$.

If the simple system (10)-(11) is compared with the exact system (6)-(7), we find that the difference between the two kinetic equations (10) and (6) lies on their right-hand sides, and their difference is of the order of unity. With the same initial condition, the error of the velocity distribution function f is of the order of $t_{m+1} - t_m$ in the interval $(t_m, t_{m+1}]$, or $\left| f - f^{\mathrm{c}} \right| = O(t_{m+1} - t_m)$, where f^{c} is the

solution of the exact kinetic system (6)-(7). Our interest is the error of the macroscopic variables ρ_r. To this end, one should note that ρ_r of the free-molecular system satisfy the conservation equations

$$\frac{\partial \rho_r}{\partial t} + \frac{\partial H_\alpha^r}{\partial x_\alpha} = 0, \tag{12}$$

and ρ_r^{c} of the exact system satisfy

$$\frac{\partial \rho_r^{\mathrm{c}}}{\partial t} + \frac{\partial H_\alpha^{r\,\mathrm{c}}}{\partial x_\alpha} = 0. \tag{13}$$

The difference between fluxes H_α^r and $H_\alpha^{r\,\mathrm{c}}$ is bounded by the difference between f and f^{c} by definition (3) and (5b), that is,

$$\left| H_\alpha^r - H_\alpha^{r\,\mathrm{c}} \right| = O\left(\left| f - f^{\mathrm{c}} \right| \right) = O(t_{m+1} - t_m), \tag{14}$$

and so, from (12) and (13),

$$\left| \rho_r - \rho_r^{\mathrm{c}} \right| = O\left((t_{m+1} - t_m)^2 \right), \tag{15}$$

in the interval $(t_m, t_{m+1}]$. Note that the error of the new Chapman-Enskog-type distribution function f^{c} also remains to be second order in $t_{m+1} - t_m$ by one time step because it is calculated from macroscopic variables. This makes the analysis continue. Thus, the error of macroscopic variables ρ_r at a finite time is of the order of $t_{m+1} - t_m$.

3. NEW LB MODEL

First, we write down the initial-value problem of the compressible NS equations:

$$\frac{\partial \rho}{\partial t} + \frac{\partial \rho u_\alpha}{\partial x_\alpha} = 0, \tag{16a}$$

$$\frac{\partial \rho u_\alpha}{\partial t} + \frac{\partial \rho u_\alpha u_\beta}{\partial x_\beta} = -\frac{\partial P_{\alpha\beta}}{\partial x_\beta}, \tag{16b}$$

$$\frac{\partial \rho (bRT + u_\alpha^2)}{\partial t} + \frac{\partial \Pi_\beta}{\partial x_\beta} = 0, \tag{16c}$$

where

$$P_{\alpha\beta} = \rho RT \delta_{\alpha\beta} - \mu \left(\frac{\partial u_\alpha}{\partial x_\beta} + \frac{\partial u_\beta}{\partial x_\alpha} - \frac{2}{3} \frac{\partial u_\chi}{\partial x_\chi} \delta_{\alpha\beta} \right) - \mu_B \frac{\partial u_\chi}{\partial x_\chi} \delta_{\alpha\beta}, \tag{17a}$$

$$\Pi_\beta = \rho\left(bRT + u_\alpha^2\right)u_\beta + 2P_{\alpha\beta}u_\alpha - 2\lambda\frac{\partial T}{\partial x_\beta}, \tag{17b}$$

with the initial condition

$$\rho = \rho^{(0)},\ u_\alpha = u_\alpha^{(0)},\ T = T^{(0)} \ \text{ at } \ t = t_0. \tag{18}$$
$$(\alpha, \beta, \chi = 1,2,\cdots,D)$$

Here t is the time, x_α is the spatial coordinate, R is the specific gas constant, and b is a given constant related to the specific-heat ratio γ by

$$\gamma = \frac{b+2}{b}. \tag{19}$$

ρ, u_α, T, $P_{\alpha\beta}$, and $\Pi_\alpha/2$ are, respectively, the density, the flow velocity in the x_α direction, the temperature, the stress tensor, and the energy flux in the x_α direction, of a gas. There are three transport coefficients: $\mu(\rho,T)$ (the viscosity), $\mu_B(\rho,T)$ (the bulk viscosity), and $\lambda(\rho,T)$ (the thermal conductivity), which are functions of ρ and T. Note that the subscripts α, β, and χ represent the number of spatial coordinates and the summation convention is applied to these subscripts.

Let us derive new LB model for the above set of compressible NS equations (16)-(18) on the basis of the discussion in Section 2. For $r = 0,1,\cdots,D+1$, we let

$$\phi_0 = 1,\ \phi_\alpha = c_\alpha,\ \phi_{D+1} = c_\alpha^2 + \eta^2. \tag{20}$$

From (16), ρ_r and $H_\alpha^{r\mathrm{c}}$ in (8) are identified as

$$\rho_0 = \rho,\ \rho_\alpha = \rho u_\alpha,\ \rho_{D+1} = \rho(bRT + u_\alpha^2), \tag{21}$$

$$H_\alpha^{0\mathrm{c}} = \rho u_\alpha,\ H_\alpha^{\beta\mathrm{c}} = \rho u_\alpha u_\beta + P_{\alpha\beta},\ H_{D+1}^{\beta\mathrm{c}} = \Pi_\beta. \tag{22}$$

To devise such a discrete-velocity scheme, the velocity distribution function f must be the collection of delta functions of c_α and η with their center at the discrete points. Let $c_{\alpha i}$ and η_i ($i = 0,1,\cdots,2I$) be such molecular velocities c_α and η on the discrete points, and f_i and f_i^{c} be the corresponding coefficients of delta functions for the velocity distribution function (i.e., $f = \sum_{i=0}^{2I} f_i\delta(c_1 - c_{1i}, c_2 - c_{2i}, \cdots, \eta - \eta_i)$) and that for the Chapman-Enskog-type distribution function, respectively. The total number of discrete molecular velocities is $2I+1$. From (2), (20), and (21), the macroscopic variables ρ, u_α, and T are defined as

$$\rho = \sum_{i=0}^{2I} f_i , \quad \rho u_\alpha = \sum_{i=0}^{2I} f_i c_{\alpha i} , \tag{23a,b}$$

$$\rho\left(bRT + u_\alpha^2\right) = \sum_{i=0}^{2I} f_i (c_{\alpha i}^2 + \eta_i^2) , \tag{23c}$$

and from (5) and (20)-(22), f_i^{c} should satisfy

$$\rho = \sum_{i=0}^{2I} f_i^{\mathrm{c}} , \quad \rho u_\alpha = \sum_{i=0}^{2I} f_i^{\mathrm{c}} c_{\alpha i} , \tag{24a,b}$$

$$\rho\left(bRT + u_\alpha^2\right) = \sum_{i=0}^{2I} f_i^{\mathrm{c}} (c_{\alpha i}^2 + \eta_i^2) , \tag{24c}$$

$$\rho u_\alpha u_\beta + P_{\alpha\beta} = \sum_{i=0}^{2I} f_i^{\mathrm{c}} c_{\alpha i} c_{\beta i} , \tag{24d}$$

$$\Pi_\beta = \sum_{i=0}^{2I} f_i^{\mathrm{c}} (c_{\alpha i}^2 + \eta_i^2) c_{\beta i} , \tag{24e}$$

where the integrals with respect to c_α and η are reduced to the summation over the discrete points because f and f^{c} are the collection of delta functions of c_α and η. There are an infinite number of particular solutions f_i^{c} of (24) and the method of solution is heuristic. In terms of computational efficiency, it is desirable that the total number of discrete molecular velocities becomes small and we present such a specific solution f_i^{c} as

$$f_i^{\mathrm{c}}\left(\rho, u_\alpha, T, \frac{\partial u_\alpha}{\partial x_\beta}, \frac{\partial T}{\partial x_\beta}\right) = \begin{cases} \dfrac{\rho bRT - P_{\alpha\alpha}}{\eta_0^2} & \text{for } i = 0, \\ -\dfrac{v_2^2}{v_1^2} F_i & \text{for } i = 1, \cdots, I, \\ \dfrac{v_1^2}{v_2^2} F_i & \text{for } i = I+1, \cdots, 2I, \end{cases} \tag{25a}$$

with

$$\begin{aligned} F_i = \frac{1}{(v_2^2 - v_1^2)(D+1)} \Bigg\{ & -\rho u_\alpha c_{\alpha i} + \frac{1}{D}\left(\frac{\rho bRT - P_{\beta\beta}}{\eta_0^2} - \rho \right) c_{\alpha i}^2 + \frac{\Pi_\beta}{v_1^2 v_2^2} c_{\beta i} c_{\alpha i}^2 \\ & + \frac{1}{v_1^2 v_2^2}\left[\frac{D+2}{2} (\rho u_\alpha u_\beta + P_{\alpha\beta}) - \frac{\rho u_\gamma^2 + P_{\gamma\gamma}}{2} \delta_{\alpha\beta} \right] c_{\alpha i} c_{\beta i} c_{\gamma i}^2 \Bigg\}, \end{aligned} \tag{25b}$$

and

$$(c_{\alpha i},\eta_i)=\begin{cases}(0,\eta_0) & \text{for } i=0,\\ (v_1 q_{\alpha i},0) & \text{for } i=1,\cdots,I,\\ (v_2 q_{\alpha i-I},0) & \text{for } i=I+1,\cdots,2I,\end{cases} \tag{26a}$$

where v_1, v_2, and η_0 are given positive constants which are chosen according to our convenience. $q_{\alpha i}$ $(i=1,\cdots,I)$ is the unit vector defined by (see Figure 1)

$$q_{\alpha i}=\begin{cases}\cos\pi i \ \ (D=1;I=2), & \left(\cos\dfrac{\pi i}{3},\sin\dfrac{\pi i}{3}\right)\ \ (D=2;I=6),\\ cyc:\dfrac{1}{5^{1/4}}\left(0,\pm\sqrt{\phi},\pm\dfrac{1}{\sqrt{\phi}}\right)\ \ (D=3;I=12),\end{cases} \tag{26b}$$

where $\phi=(1+\sqrt{5})/2$ and *cyc* represents cyclic permutation. Now, new LB model for the set of the compressible NS equations (16)-(18) is arranged simply in the following way.

1. Set $\rho^{(0)}$, $u_\alpha^{(0)}$, and $T^{(0)}$ as the initial values of ρ, u_α, and T at $t=t_0$, and compute $f_i^{\mathrm{c}}\left(\rho^{(0)},u_\alpha^{(0)},T^{(0)},\partial u_\alpha^{(0)}/\partial x_\beta,\partial T^{(0)}/\partial x_\beta\right)$.
2. Solve the discrete-type free-molecular kinetic equation for f_i $(i=0,1,\cdots,2I)$

$$\frac{\partial f_i}{\partial t}+c_{\alpha i}\frac{\partial f_i}{\partial x_\alpha}=0, \tag{27}$$

(method of spatial discretization is explained in the first paragraph of Section 4) in a continuous sequence of time intervals $(t_0,t_1]$, $(t_1,t_2],\cdots$ under the following initial condition for each interval $(t_m,t_{m+1}]$ from $m=0$:

$$f_i=f_i^{\mathrm{c}}\left(\rho^{(m)},u_\alpha^{(m)},T^{(m)},\frac{\partial u_\alpha^{(m)}}{\partial x_\beta},\frac{\partial T^{(m)}}{\partial x_\beta}\right), \tag{28}$$

where f_i^{c} and $c_{\alpha i}$ are defined by (25) and (26), respectively. It should be noted that the viscosities μ and μ_B and the thermal conductivity λ included in $P_{\alpha\beta}$ and Π_β defined by (17) can be chosen freely according to our convenience.

Then the macroscopic variables ρ, u_α, and T obtained from the solution f_i at an arbitrary time satisfy the compressible NS equations, or (16) within the error of $O(t_{m+1}-t_m)$ which can be made sufficiently small irrespective of flow parameters.

It is evident that the proposed LB model (27)-(28) given above overcomes the difficulties (i) and (ii), since the error proportional to flow parameters does not arise, and any parameters including three transport coefficients μ, μ_B, and λ are chosen freely. Thus, our proposed model can give solution

of the compressible NS equations for 'any' parameter sets as accurately as possible only if the time interval $t_{m+1} - t_m$ is taken to be sufficiently small.

4. NUMERICAL TESTS AND ERROR ESTIMATES

In this section, we will conduct several numerical tests of the LB model (27)-(28) presented in Section 3 and estimate their errors. The finite-difference scheme with the usual first-order forward in time and the third-order upwind in space (so called UTOPIA) is used for numerical computation of the kinetic equation (27). The first derivatives of macroscopic variables included in f_i^{c} (see (25)) are evaluated by the second-order centered differences. For all the numerical computation, the mesh widths for t and x_α are set to be different constant values Δt and Δx_α, respectively.

4.1. Propagation of expansion waves

We first treat the expansion-wave problem, that is, the one-dimensional initial-value problem of (16)-(18) with $D = 1$ whose initial macroscopic variables at $t = 0$ are given by

$$\rho^{(0)} = \rho_0, \quad u_1^{(0)} = U \tanh(x_1 / L), \quad T^{(0)} = T_0, \tag{29}$$

where ρ_0, U, L, and T_0 are given positive constants. This problem is characterized by the specific-heat ratio γ (see (19)), the Mach number Ma, the Reynolds number Re, and the Prandtl number Pr defined by

$$\mathrm{Ma} = \frac{U}{\sqrt{\gamma R T_0}}, \quad \mathrm{Re} = \frac{\rho_0 U L}{\mu(\rho_0, T_0)}, \quad \mathrm{Pr} = \frac{(b+2) R \mu(\rho_0, T_0)}{2\lambda(\rho_0, T_0)}, \tag{30}$$

as well as the functional forms of $\mu(\rho, T)$ and $\lambda(\rho, T)$ (μ_B is incorporated into μ for $D = 1$). Numerical results at $\hat{t} \equiv t\sqrt{RT_0} / L = 20$ for $\gamma = 5/3$, $\mathrm{Ma} = 0.5$, $\mathrm{Re} = 10$, and three different values of $\mathrm{Pr} = 0.01$, 0.1, and 1 with μ and λ being constants are shown in Figure 2. The symbols represent results by the proposed model (27)-(28) with $D = 1$ while the solid lines are the corresponding numerical results of the NS equations themselves (16)-(18) solved by the so-called MacCormack scheme [28]. We find a good agreement between the two results. There are several existing models that can compute the Prandtl number other than unity [11,12,29,30], but as far as we know there are no models yet that can determine 'functional forms' of three transport coefficients μ, μ_B and λ freely.

Let us consider the above expansion-wave problem when λ is not constant. Temperature fields at $\hat{t} = 20$ calculated from the proposed LB model (27)-(28) with $D = 1$ are plotted in Figure 3 by the symbols together with the corresponding results of the NS equations solved by the MacCormack scheme (represented by the solid line). We find a good agreement between the two results for each case, or $\lambda(\rho,T)/\lambda(\rho_0,T_0) = T/T_0$, $(T/T_0)^3$, and $(T/T_0)^5$ with constant μ, so that the issue (ii) is resolved completely.

The error of the numerical scheme [31] is now defined as

$$Er = \frac{\int_{-\infty}^{\infty} \left| u_1 - u_1^{\mathrm{exa}} \right| dx_1}{\sqrt{\gamma R T_0}\, L}, \tag{31}$$

where the variable with the superscript 'exa' represents the exact solution of the set of the compressible NS equations (16)-(18). Here we used numerical solution by the MacCormack method with sufficient number of meshes as the exact solution. In Figure 4, Er for the proposed LB model and that for the existing model [8] are plotted as functions of the dimensionless time increment $\Delta\hat{t} \equiv \sqrt{RT_0}\,\Delta t / L$. Here $\mathrm{Pr} = 1$ with constant μ and λ are chosen in order to make a comparison with the existing model possible. One finds that Er for the current existing model asymptotes to some nonzero value proportional to $(\mathrm{Ma}/\mathrm{Re})^2$ as $\Delta\hat{t}$ decreases. This is the error inherent to the LBM which was described as the issue (i) in Section 1 of this paper. In contrast, Er for the new model approaches zero as $\Delta\hat{t}$ decreases, or $Er \to 0$ as $\Delta\hat{t} \to 0$ so that this issue (i) is overcome in the proposed model.

4.2. Shock-tube problem

In this section, we consider the shock-tube problem. The initial macroscopic variables are given by

$$\rho^{(0)} = \frac{\rho_0 + \rho_1 + (\rho_1 - \rho_0)\tanh(x_1/L)}{2}, \quad u_1^{(0)} = 0, \quad T^{(0)} = T_0, \tag{32}$$

where ρ_0, ρ_1, L, and T_0 are given positive constants. This problem is characterized by ρ_1/ρ_0, γ, $\mathrm{Re/Ma}$, Pr, and the functional forms of μ and λ. Numerical results at $\hat{t} = 20$ for $\rho_1/\rho_0 = 2$, $\gamma = 1.4$, $\mathrm{Re/Ma} = 10$, and three different values of $\mathrm{Pr} = 0.01$, 0.1, and 1 with constant μ and λ are shown in Figure 5 by the symbols. Numerical results of the NS equations solved by the MacCormack scheme are represented by the solid lines. We find a good agreement between the two results.

The error estimate is presented in Figure 6. In the expansion-wave problem presented in Section 4.1, where the shock wave does not appear, Er for the existing LB model asymptotes to the value proportional to $(\mathrm{Ma}/\mathrm{Re})^2$ as $\Delta\hat{t}$ decreases, while in the present problem where the shock wave

appears, it asymptotes to different constant values proportional to Ma/Re as shown by the dashed lines in Figure 6. For our proposed new model, however, Figure 6 shows that Er always approaches zero as $\Delta\hat{t} \to 0$ irrespective of appearance of shock waves as shown by the solid lines.

4.3. Couette flows

We next show results of the two-dimensional steady Couette flows. The boundary conditions are

$$u_1 = -U, \quad T = T_0 \quad \text{at} \quad x_2 = -L, \tag{33a}$$

$$u_1 = U, \quad T = T_0 \quad \text{at} \quad x_2 = L, \tag{33b}$$

where U, T_0 and L are given positive constants. These boundary conditions can be readily applied by fixing the values of $u_1^{(m)}$ and $T^{(m)}$ in (28) at $\pm U$ and T_0 on the spatial mesh points corresponding to $x_2 = \pm L$. This problem is characterized by a single parameter $(\gamma - 1)\mathrm{Ma}^2\,\mathrm{Pr}$ and the functional forms of μ and λ. Temperature fields for $(\gamma - 1)\mathrm{Ma}^2\,\mathrm{Pr} = 2$ and three different functional forms of $\mu(\rho, T)/\mu(\rho_0, T_0) = 1$, $(T/T_0)^{1/2}$ and T/T_0 with constant λ are shown in Figure 7. The symbols represent those calculated from the new model (27)-(28) with $D = 2$, while the solid lines are the corresponding numerical results of the NS equations solved by the MacCormack scheme. We find a good agreement between the two results.

4.4. Transonic flow around NACA 0012 airfoil

In order to validate our proposed model to actual flows, we also treated rather practical test problem, a flow around NACA 0012 airfoil [32-35]. Non-slip boundary conditions are imposed on the surface of airfoil and a uniform flow with constant density and temperature is prescribed at far field. This problem is characterized by the Mach number Ma of uniform flow, its angle α of attack, the Reynolds number Re (based on the chord length), the Prandtl number Pr of fluid and its specific-heat ratio γ.

Numerical results for Ma=0.8, $\alpha = 10^\circ$, Re=500, Pr=0.72, $\gamma = 1.4$ are presented in Figure 8. We utilized the O-type grid with 250 points on the airfoil and 250 points in the radial direction, and the far-field boundary is located at the radius of 35 times that of a chord length. Figure 8(a) shows the streamline pattern, and one can observe the well-known feature of the flow, that is, appearance of a vortex region along the upper surface of the airfoil. The comparison of pressure coefficient and skin friction coefficient distributions on the airfoil surface is presented in Figures 8(b,c), and we see good agreement between the results of our model and those by Jawahar and Kamath [32]. The drag and lift coefficients are compared in Table 1, and our results are well within the range reported in the literature

[32-34].

4.5. Flow around a cylinder (Aeolian tone)

We also tested flow around a cylinder. This flow is associated with production and propagation of aerodynamic sound (aeolian tone). So we can check applicability of our model to the flow associated with production of aerodynamic sound [36-38], which is one of strength of LBM as mentioned in the first paragraph of Section 1. The boundary conditions on the cylinder are non-slip conditions and those at far field are uniform flow with constant density and temperature. In this test, the far-field boundary is located sufficiently far from the cylinder, at 300 times that of the cylinder diameter, in order to examine features of sound wave clearly. This problem is characterized by the Mach number Ma, the Reynolds number Re (based on diameter L of cylinder), the Prandtl number Pr and the specific-heat ratio γ. The latter two parameters are fixed at Pr=0.66 and $\gamma = 1.4$.

Figure 9(a) shows pressure distribution for Ma=0.3 and Re=150 over a relatively wide domain ($-170L < x, y < 170L$) centered at the cylinder. Although the pressure deviation due to propagation of sound wave is quite small, our model captures its behavior surprisingly well. In order to make quantitative comparison, we also give in figure 9(b) the pressure distribution along the y axis passing through the center of cylinder. Sound wave amplitude, or the amplitude of pressure oscillation can be seen to decay in inverse proportion to $y^{1/2}$, and agree well with the far-field linear theory by Curle [39-41]:

$$\frac{p - p_\infty}{p_\infty} = 0.057 \frac{\rho_\infty c_\infty^2}{p_\infty} \frac{\mathrm{Ma}^{5/2}}{(y/L)^{1/2}}, \tag{34}$$

where the quantities with subscript ∞ are evaluated at far field and c is the sound speed. Finally, we show in figure 9(c) comparison of the Strouhal number obtained by our proposed model and that reported in Williamson & Brown [42]. As can be seen from this figure, the results of our model agree well with that reported in the literature for wide range of the Reynolds numbers.

5. CONCLUSION

We have presented a new type of lattice Boltzmann model that gives solution of the compressible NS equations on the basis of the kinetic system developed by Sone. This model overcomes the remaining issues (i) and (ii) and several other shortcomings on the computational efficiency of current LBM which are mentioned in Section 1. Numerical examples and specific error estimates are also given for

simple test cases in order to support the above statements. To validate our model for flows with complex geometry, we also treated the flow past NACA 0012 airfoil and see good agreement with well-established solutions. We also conducted simulation of flows past a cylinder to evaluate its ability to capture propagation of sound wave and again find good agreement with previous results and theory. Since our model is very simple in its numerical scheme, it can be a good alternative to current LBM models.

ACKNOWLEDGEMENTS

We thank Professor Yoshio Sone and anonymous referees for their valuable comments on the manuscript. This work was partially supported by a Grant-in-Aid for Scientific Research from the Ministry of Education, Science and Culture (No. 18K03930).

REFERENCES

1. Alexander FJ, Chen S, Sterling JD. Lattice Boltzmann thermohydrodynamics. *Physical Review E* 1993; **47**: R2249-2252.
2. Qian Y. Simulating thermohydrodynamics with lattice BGK models. *Journal of Scientific Computing* 1993; **8**(3): 231-242.
3. Chen Y, Ohashi H, Akiyama H. Thermal lattice Bhatnagar-Gross-Krook model without nonlinear deviations in macrodynamic equations. *Physical Review E* 1994; **50**: 2776-2783.
4. Chen S, Doolen GD. Lattice Boltzmann method for fluid flows. *Annual Review of Fluid Mechanics* 1998; **30**: 329-364.
5. Sun C. Lattice-Boltzmann models for high speed flows. *Physical Review E* 1998; **58**(6):7283–7287.
6. Sun C. Adaptive lattice Boltzmann model for compressible flows: viscous and conductive properties. *Physical Review E* 2000; **61**(3):2645–2653.
7. Shi W, Shyy W, Mei R. Finite-difference-based lattice Boltzmann method for inviscid compressible flows. *Numerical Heat Transfer: Part B: Fundamentals* 2001; **40**(1):1–21.
8. Kataoka T, Tsutahara M. Lattice Boltzmann model for the compressible Navier-Stokes equations with flexible specific-heat ratio. *Physical Review E* 2004; **69**: 035701(R).
9. Kataoka T, Tsutahara M. Lattice Boltzmann method for the compressible Euler equations. *Physical Review E* 2004; **69**: 056702.
10. He X, Chen S, Doolen GD. A novel thermal model for the lattice Boltzmann method in

incompressible limit. *Journal of Computational Physics* 1998; **146**: 282-300.

11. Li Q, He YL, Wang Y, Tao WQ. Coupled double-distribution-function lattice Boltzmann method for the compressible Navier-Stokes equations. *Physical Review E* 2007; **76**: 056705.
12. Qu K, Shu C, Chew YT. Alternative method to construct equilibrium distribution functions in lattice-Boltzmann method simulation of inviscid compressible flows at high Mach number. *Physical Review E* 2007; **75**: 036706.
13. Tosi F, Ubertini S, Succi S, Chen H, Karlin IV. Numerical stability of entropic versus positivity-enforcing lattice Boltzmann schemes. *Mathematics and Computers in Simulation* 2006; **72**: 227-231.
14. Ansumali S, Karlin IV. Entropy function approach to the lattice Boltzmann method. *Journal of Statistical Physics* 2002; **107**: 291-308.
15. Li Y, Shock R, Zhang R, Chen H. Numerical study of flow past an impulsively started cylinder by the lattice-Boltzmann method. *Journal of Fluid Mechanics* 2004; **519**: 273-300.
16. Pan XF, Xu A, Zhang G, Jiang S. Lattice Boltzmann approach to high-speed compressible flows *International Journal of Modern Physics C* 2007; **18**: 1747-1764.
17. Gan Y, Xu A, Zhang G, Yu X, Li Y, Two-dimensional lattice Boltzmann model for compressible flows with high Mach number. *Physica A* 2008; **387**: 1721-1732.
18. Brownlee RA, Gorban AN, Levesley J. Stability and stabilization of the lattice Boltzmann method. *Physical Review E* 2007; **75**: 036711.
19. Gan YB, Xu AG, Zhang GC, Li YJ. Flux limiter lattice Boltzmann scheme approach to compressible flows with flexible specific-heat ratio and Prandtl number. *Communications in Theoretical Physics* 2011; **56**(9): 490–498.
20. Chen F, Xu AG, Zhang GC, Li YJ, Succi S. Multiple-relaxation-time lattice Boltzmann approach to compressible flows with flexible specific-heat ratio and Prandtl number. *Europhysics Letters.* 2010; **90**(5): 54003.
21. Chen F, Xu A, Zhang GC, Li YJ. Multiple-relaxation-time lattice Boltzmann model for compressible fluids. *Physics Letters. A* 2011; **375**(21): 2129–2139.
22. Gan YB, Xu A, Zhang GC, Yang Y. Lattice BGK kinetic model for high speed compressible flows: hydrodynamic and nonequilibrium behaviors. *Europhysics letters* 2013; **103**(2): 330–337.
23. Sone Y. *Kinetic Theory and Fluid Dynamics*. Birkhäuser: Boston, 2002.
24. Pullin DI. Direct simulation methods for compressible inviscid ideal-gas flow. *Journal of Computational Physics* 1980; **34**: 231-244.
25. Chou SY, Baganoff D. Kinetic Flux–Vector Splitting for the Navier–Stokes Equations. *Journal of Computational Physics* 1997; **130**: 217-230.

26. Junk M, Rao SVR. A new discrete velocity method for Navier-Stokes equations. *Journal of Computational Physics* 1999; **151**: 178-198.
27. Inamuro T. A lattice kinetic scheme for incompressible viscous flows with heat transfer. *Philosophical Transactions of the Royal Society of London A* 2002*;* **360**: 477-484.
28. MacCormack RW. The effect of viscosity in hypervelocity impact cratering. *AIAA Paper* 1969; **69**-354.
29. Prasianakis NI, Karlin IV. Lattice Boltzmann method for simulation of compressible flows on standard lattices. *Physical Review E* 2007; **78**: 016704.
30. Li K, Zhong C. A lattice Boltzmann model for simulation of compressible flows. *International Journal for Numerical Methods in Fluids* 2015; **77**: 334–357.
31. Kataoka T, Tsutahara M. Accuracy of the lattice Boltzmann method for describing the behavior of a gas in the continuum limit. *Physical Review E* 2010; **82**: 056709.
32. Jawahar P, Kamath H. A high-resolution procedure for Euler and Navier–Stokes computations on unstructured grids. *Journal of Computational Physics* 2000; **164**: 165-203.
33. Bristeau MO, Glowinski R, Periaux J, Viviand H. *Numerical simulation of compressible Navier-Stokes flows*. Vieweg and Sonh Braunschweig: Wiesbaden, 1987.
34. Yang LM, Shu C, Wu J. A hybrid lattice Boltzmann flux solver for simulation of viscous compressible flows. *Advances in Applied Mathematics and Mechanics* 2016; **8**: 887-910.
35. Yang LM, Shu C, Wang Y. Development of a discrete gas-kinetic scheme for simulation of two-dimensional viscous incompressible and compressible flows. *Physical Review E* 2016; **93**: 033311.
36. Tsutahara M, Kurita M, Kataoka T. Direct simulation of aerodynamic sound by finite-difference lattice Boltzmann method. *Transactions of the Japan Society of Mechanical Engineers Series B* 2003; 69: 841-847 (in Japanese).
37. Tsutahara M, Kataoka T, Shikata K, Takada N. New model and scheme for compressible fluids of the finite difference lattice Boltzmann method and direct simulations of aerodynamic sound. *Computers and Fluids* 2008; **37**: 79-89.
38. Tamura A, Tsutahara M, Kataoka T, Aoyama T, Yang C. Numerical simulation of two-dimensional blade-vortex interactions using finite difference lattice Boltzmann method. *AIAA Journal* 2008; **46**: 2235-2247.
39. Curle N. The influence of solid boundaries upon aerodynamic sound. *Proc. R. Soc. Lond. A* 1955; **231**, 505-514.
40. Inoue O, Hatakeyama N. Sound generation by a two-dimensional circular cylinder in a uniform flow. *J. Fluid Mech.* 2002; **471**, 285-314.

41. Nishioka M, Sakaue S. Vortex pair and vortex ring as flow models for Aeolian tones. *Journal of Japan Society of Fluid Mechanics 'Nagare'* 2005; **24**: 105-113 (in Japanese).
42. Williamson CHK, Brown GL. A series in $1/\sqrt{\mathrm{Re}}$ to represent the Strouhal-Reynolds number relationship of the cylinder wake. *Journal of Fluids and Structures* 1998; **12**: 1073-1085.

FIGURE CAPTIONS

Figure 1 Distribution of the unit vector $q_{\alpha i}$ ($\alpha = 1,\cdots,D$; $i = 0,\cdots,I$): (a) one-dimensional model ($D = 1$, $I = 2$); (b) two-dimensional model ($D = 2$, $I = 6$); (c) three-dimensional model ($D = 3$, $I = 12$).

Figure 2 Numerical results $u_1/\sqrt{\gamma RT_0}$ and T/T_0 at $\hat{t} = 20$ for the expansion-wave problem whose initial condition is (29), when $\gamma = 5/3$, $\mathrm{Ma} = 0.5$, $\mathrm{Re} = 10$, and $\mathrm{Pr} = 0.01$, 0.1, 1 (μ and λ are constants). The symbols (○, $\mathrm{Pr} = 0.01$; △, $\mathrm{Pr} = 0.1$; □, $\mathrm{Pr} = 1$) are the results by the proposed model (27)-(28) with $D = 1$ and $(v_1, v_2, \eta_0)/\sqrt{RT_0} = (1.3, 2.1, 3)$, and the lines are the corresponding results by the MacCormack method. From the symmetry of the problem with respect to $x_1 = 0$, only the results for $x_1 > 0$ are shown.

Figure 3 Temperature fields T/T_0 at $\hat{t} = 20$ for the expansion-wave problem whose initial condition is (29), when $\gamma = 5/3$, $\mathrm{Ma} = 0.5$, $\mathrm{Re} = 10$, $\mathrm{Pr} = 0.01$, and $\lambda(\rho,T)/\lambda(\rho_0,T_0) = T/T_0$, $(T/T_0)^3$, $(T/T_0)^5$ (μ is constant). The symbols (○, $\lambda(\rho,T)/\lambda(\rho_0,T_0) = T/T_0$; △, $(T/T_0)^3$; □, $(T/T_0)^5$) are the results by the proposed model, and the lines are the corresponding results by the MacCormack method.

Figure 4 Error Er of numerical results at $\hat{t} = 20$ versus dimensionless time increment $\Delta\hat{t}$ for the expansion-wave problem whose initial condition is (29), when $\gamma = 5/3$, $\mathrm{Ma} = 0.5$, $\mathrm{Pr} = 1$, and $\mathrm{Re} = 5$, 10, 30 (μ and λ are constants). The symbols (○, Re=5; △, Re=10; □, Re=30) connected by solid lines represent results by the proposed model and the crosses connected by dashed lines are those by the existing model [8].

Figure 5 Numerical results $u_1/\sqrt{\gamma RT_0}$ and T/T_0 at $\hat{t} = 20$ for the shock-tube problem whose initial condition is (32), when $\rho_1/\rho_0 = 2$, $\gamma = 1.4$, $\mathrm{Re}/\mathrm{Ma} = 10$, and $\mathrm{Pr} = 0.01$, 0.1, 1 (μ and λ are constants). The symbols (○, $\mathrm{Pr} = 0.01$; △, $\mathrm{Pr} = 0.1$; □, $\mathrm{Pr} = 1$) are the results by the proposed scheme, and the lines are the corresponding results by the MacCormack method.

Figure 6 Error Er of numerical results at $\hat{t} = 20$ versus dimensionless time increment $\Delta\hat{t}$ for the shock-tube problem whose initial condition is (32), when $\rho_1/\rho_0 = 2$, $\gamma = 1.4$, $\mathrm{Pr} = 1$, and $\mathrm{Re}/\mathrm{Ma} = 5,\ 10,\ 30$ (μ and λ are constants). The symbols (○, Re/Ma=5; △, Re/Ma=10; □, Re/Ma=30) connected by solid lines represent results by the proposed model and the crosses connected by dashed lines are those by the existing model [8].

Figure 7 Numerical results u_1/U and T/T_0 for the two-dimensional steady Couette flow problem whose boundary conditions are (33), when $(\gamma - 1)\mathrm{Ma}^2\,\mathrm{Pr} = 2$ and $\mu(\rho,T)/\mu(\rho_0,T_0) = 1$, $(T/T_0)^{1/2}$, T/T_0 (λ is constant). The symbols (○, $\mu(\rho,T)/\mu(\rho_0,T_0) = 1$; △, $(T/T_0)^{1/2}$; □, T/T_0) are the results by the proposed model. The solid lines are the corresponding results by the MacCormack method.

Figure 8 Numerical results for flow around NACA0012 airfoil for Ma=0.8, $\alpha = 10^\circ$, Re=500, Pr=0.72 and $\gamma = 1.4$: (a) Streamline pattern obtained by the proposed model. (b) Comparison of pressure coefficient distribution C_p obtained by our model and that reported by Jawahar & Kamath [32]. Following the convention of the above literature, the ordinate is reversed. (c) Comparison of skin friction coefficient distribution C_f.

Figure 9 Numerical results for flow around a cylinder (Pr=0.66 and $\gamma = 1.4$): (a) Pressure distribution for Ma=0.3 and Re=150 obtained by the proposed model over a wide domain ($-170L < x, y < 170L$) centered at cylinder. (b) Pressure distribution along the y axis for Re=150 obtained by the proposed model (black and red solid lines). The dashed lines are the theory (34) by Curle for the envelop amplitudes. (c) Comparison of Strouhal numbers for Ma=0.3 obtained by the proposed model (○) and those reported by Williamson & Brown [42] (solid line).

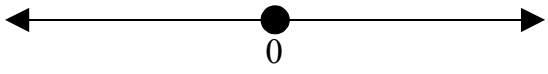

(a)

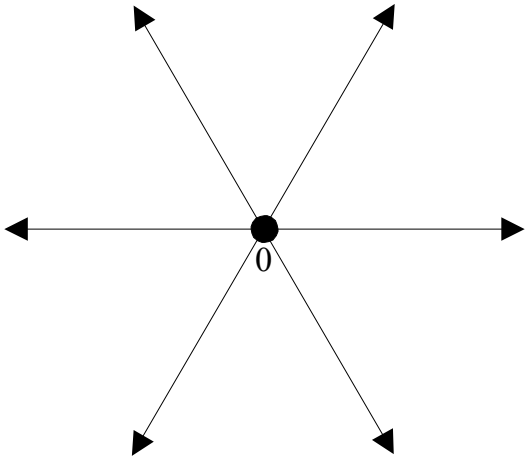

(b)

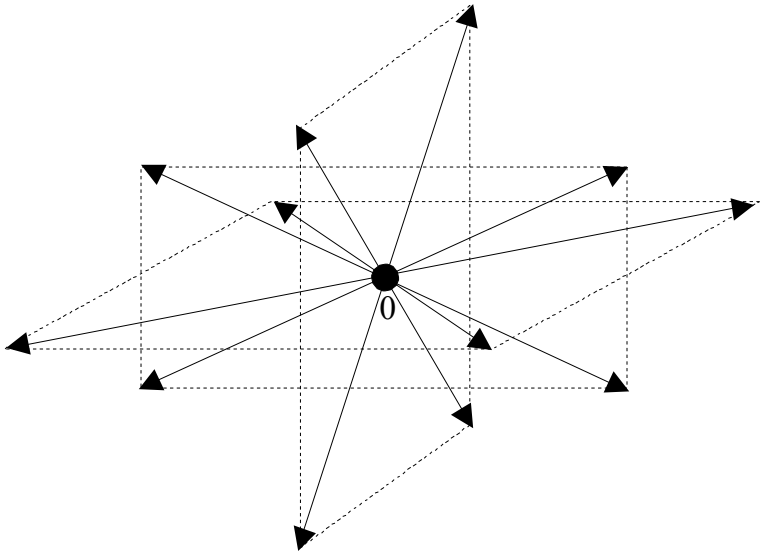

(c)

Figure 1

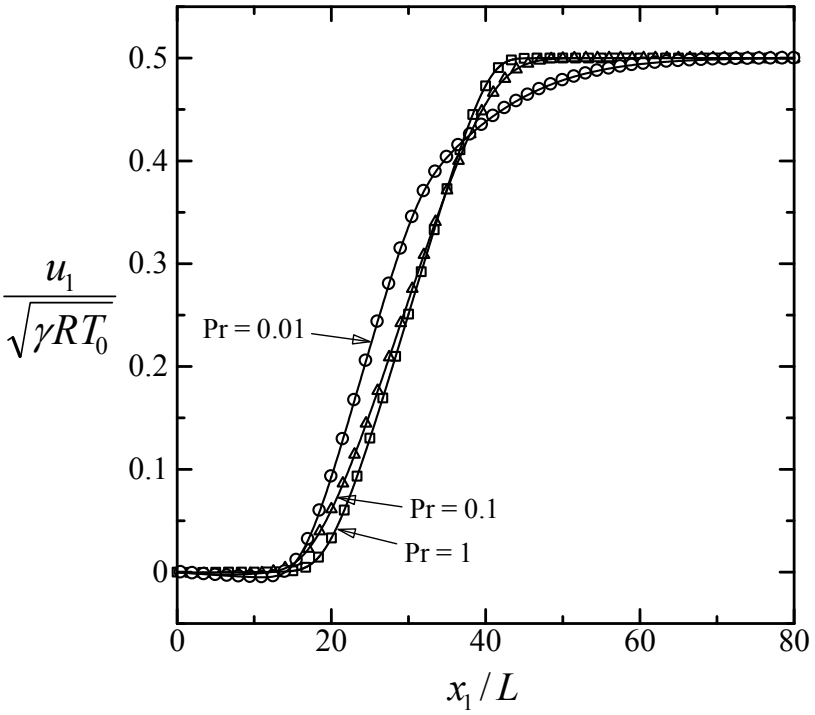
$\frac{u_1}{\sqrt{\gamma R T_0}}$
0.5
0.4
0.3
0.2
0.1
0
Pr = 0.01
Pr = 0.1
Pr = 1
0
20
40
60
80
x_1 / L

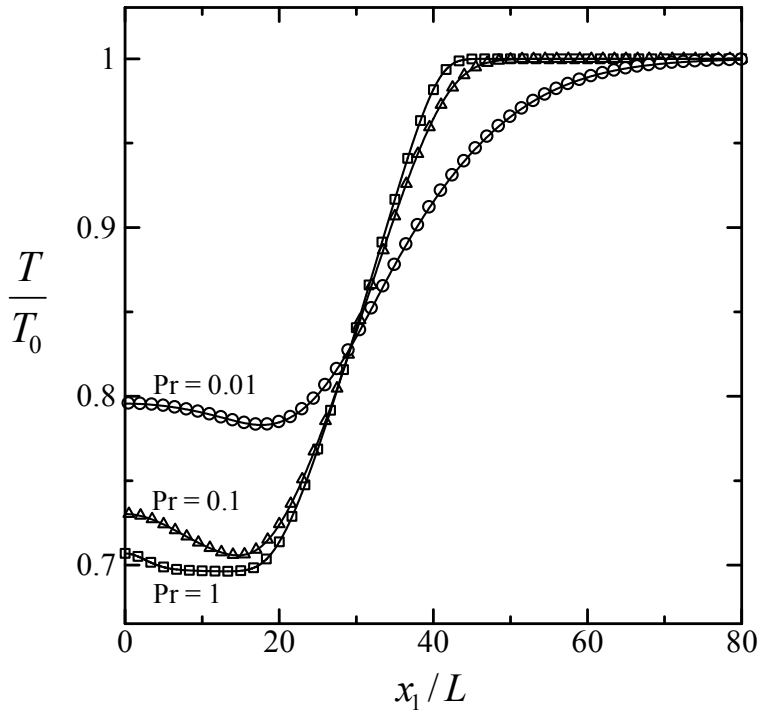
$\frac{T}{T_0}$
1
0.9
0.8
0.7
Pr = 0.01
Pr = 0.1
Pr = 1
0
20
40
60
80
x_1 / L

Figure 2

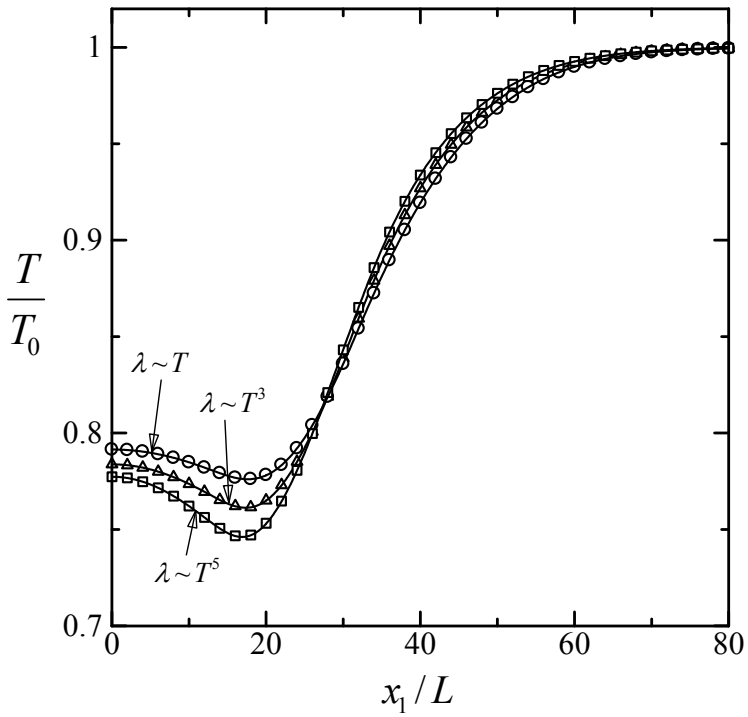
1
0.9
0.8
0.7
$\frac{T}{T_0}$
$\lambda \sim T$
$\lambda \sim T^3$
$\lambda \sim T^5$
0
20
40
60
80
x_1 / L

Figure 3

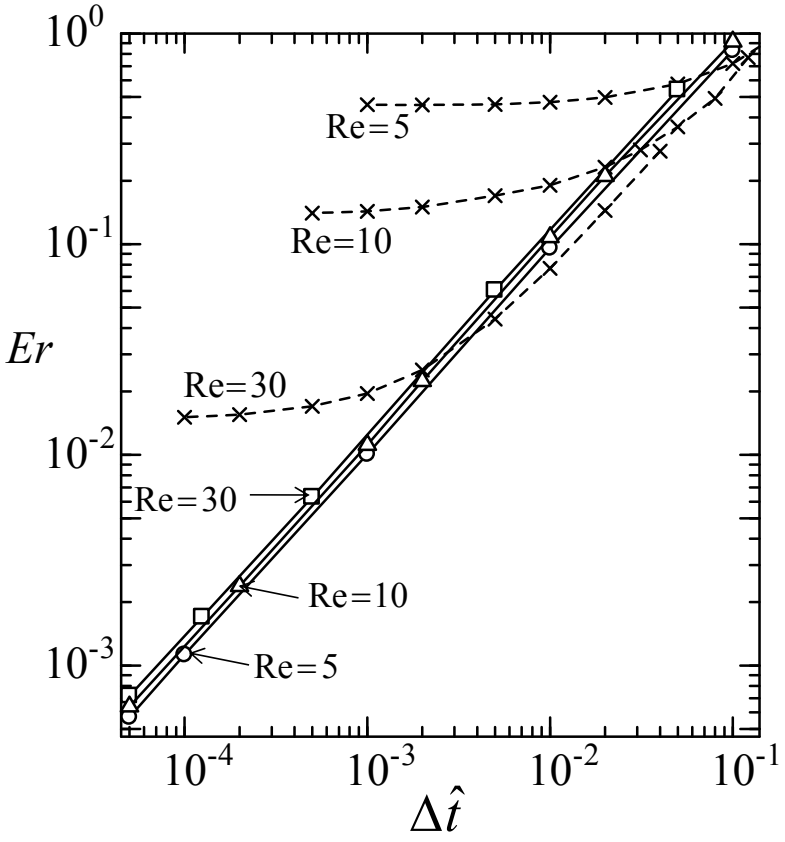
10^0
10^{-1}
10^{-2}
10^{-3}
Er
Re=5
Re=10
Re=30
Re=30
Re=10
Re=5
10^{-4}
10^{-3}
10^{-2}
10^{-1}
$\Delta\hat{t}$

Figure 4

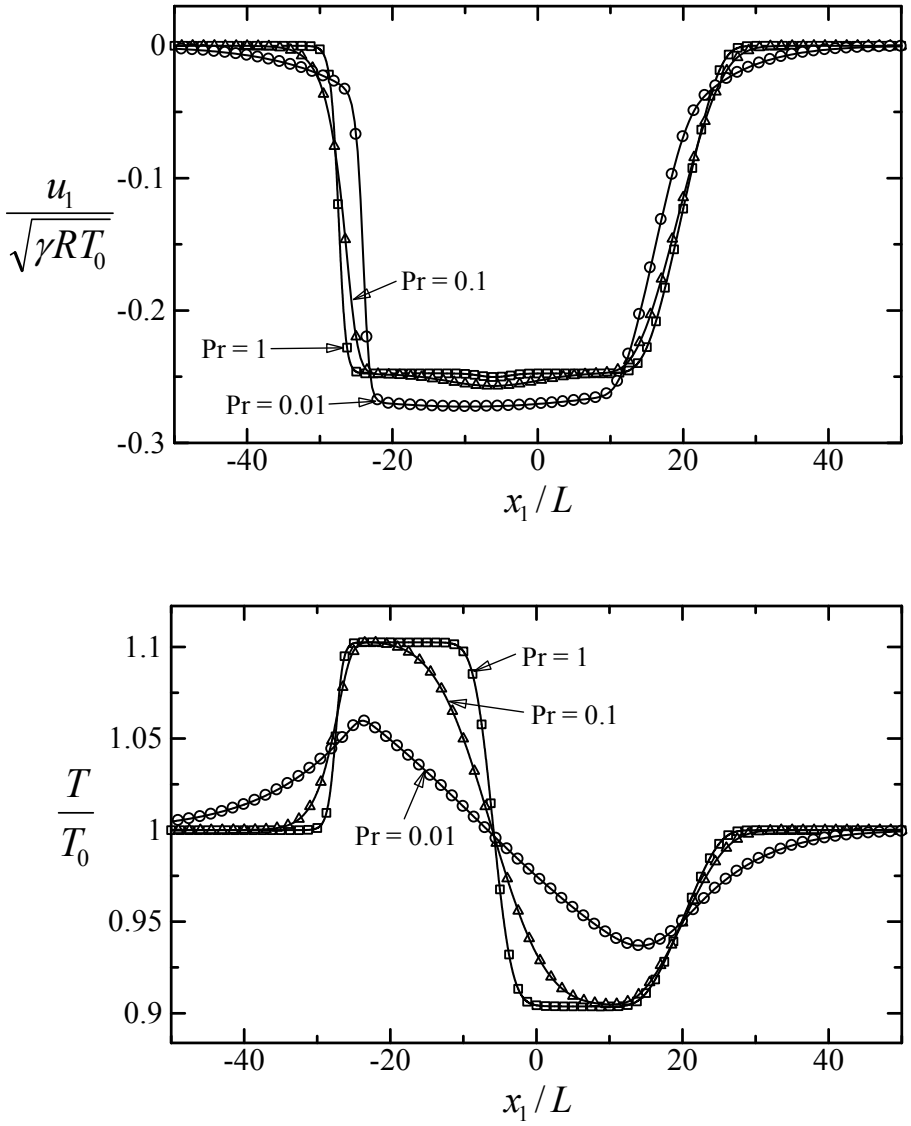
$\frac{u_1}{\sqrt{\gamma R T_0}}$
0
-0.1
-0.2
-0.3
Pr = 0.1
Pr = 1
Pr = 0.01
-40
-20
0
20
40
x_1 / L
$\frac{T}{T_0}$
1.1
1.05
1
0.95
0.9
Pr = 1
Pr = 0.1
Pr = 0.01
-40
-20
0
20
40
x_1 / L

Figure 5

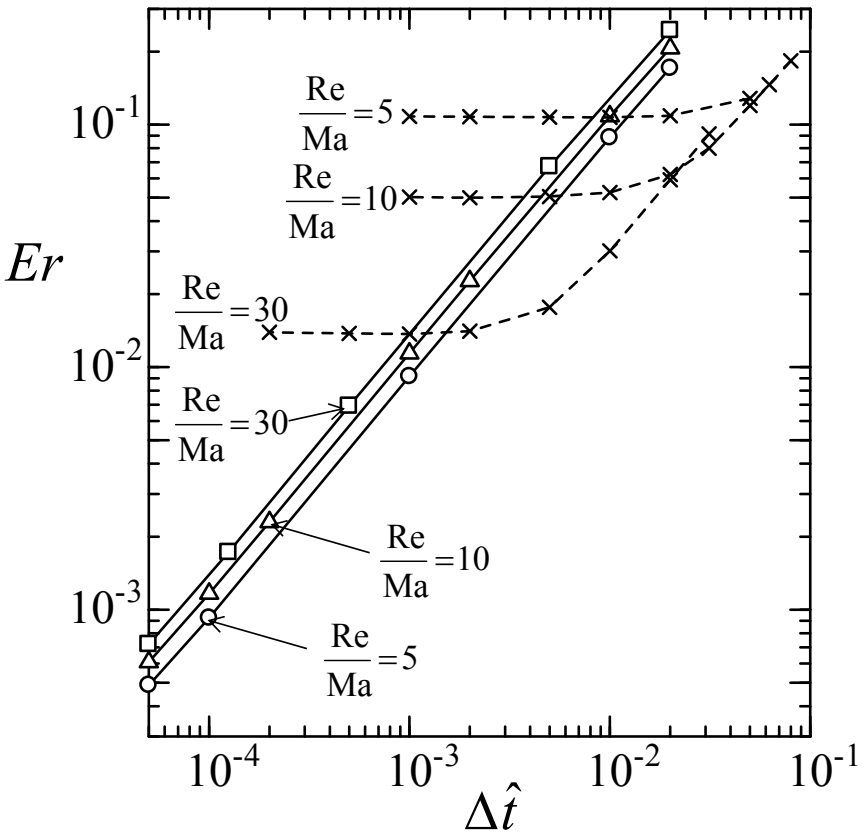
Er
10^{-1}
10^{-2}
10^{-3}
10^{-4}
10^{-3}
10^{-2}
10^{-1}
$\Delta\hat{t}$
$\frac{\mathrm{Re}}{\mathrm{Ma}}=5$
$\frac{\mathrm{Re}}{\mathrm{Ma}}=10$
$\frac{\mathrm{Re}}{\mathrm{Ma}}=30$
$\frac{\mathrm{Re}}{\mathrm{Ma}}=30$
$\frac{\mathrm{Re}}{\mathrm{Ma}}=10$
$\frac{\mathrm{Re}}{\mathrm{Ma}}=5$

Figure 6

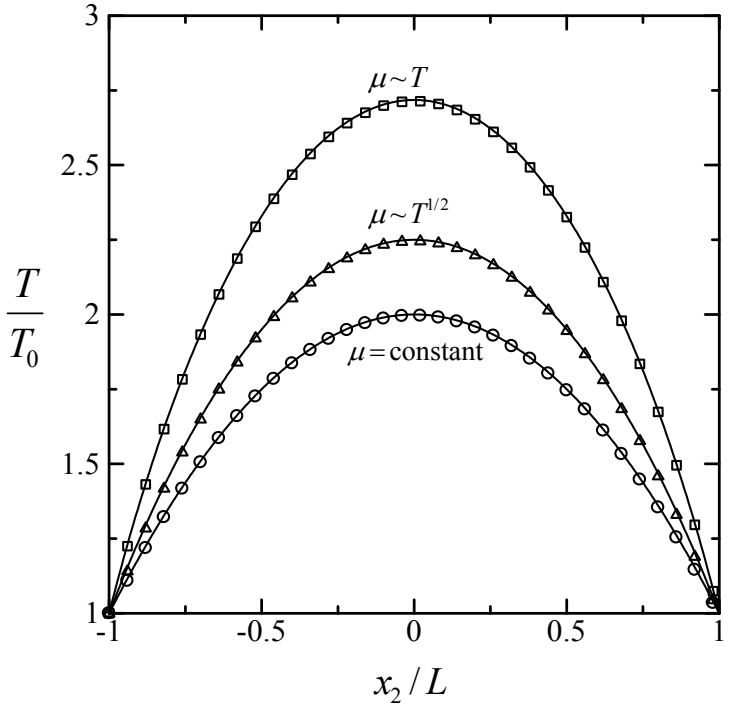

Figure 7

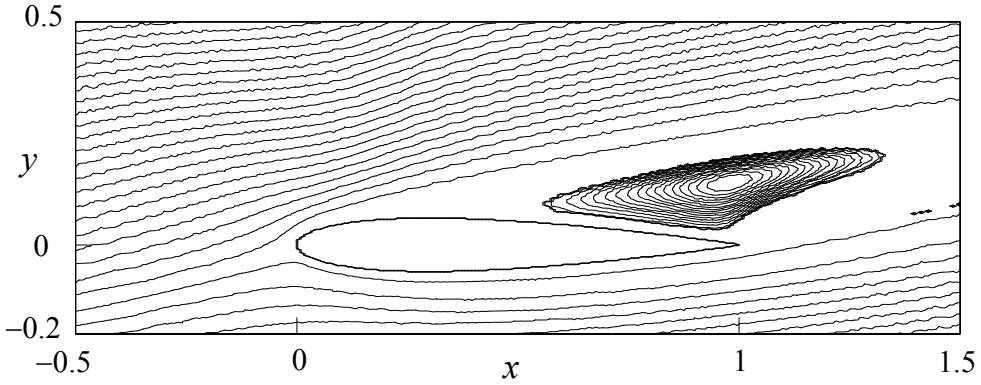

(a)

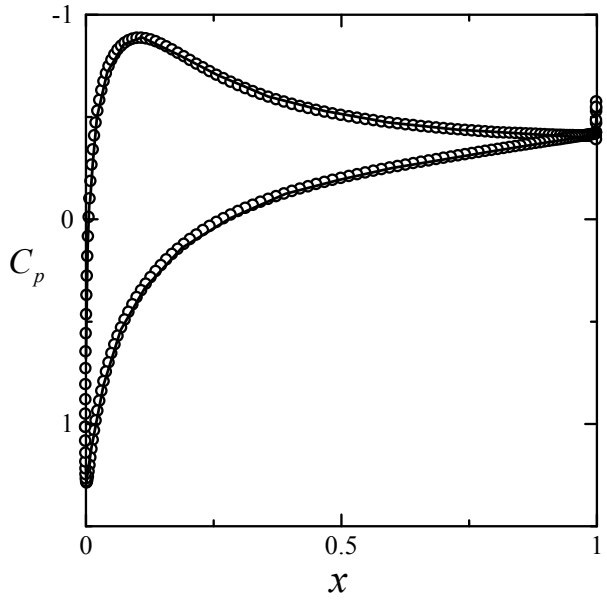

(b)

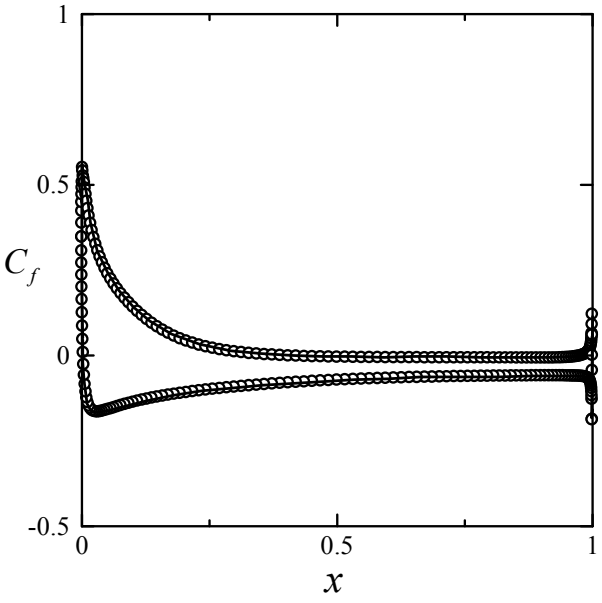

(c)

Figure 8

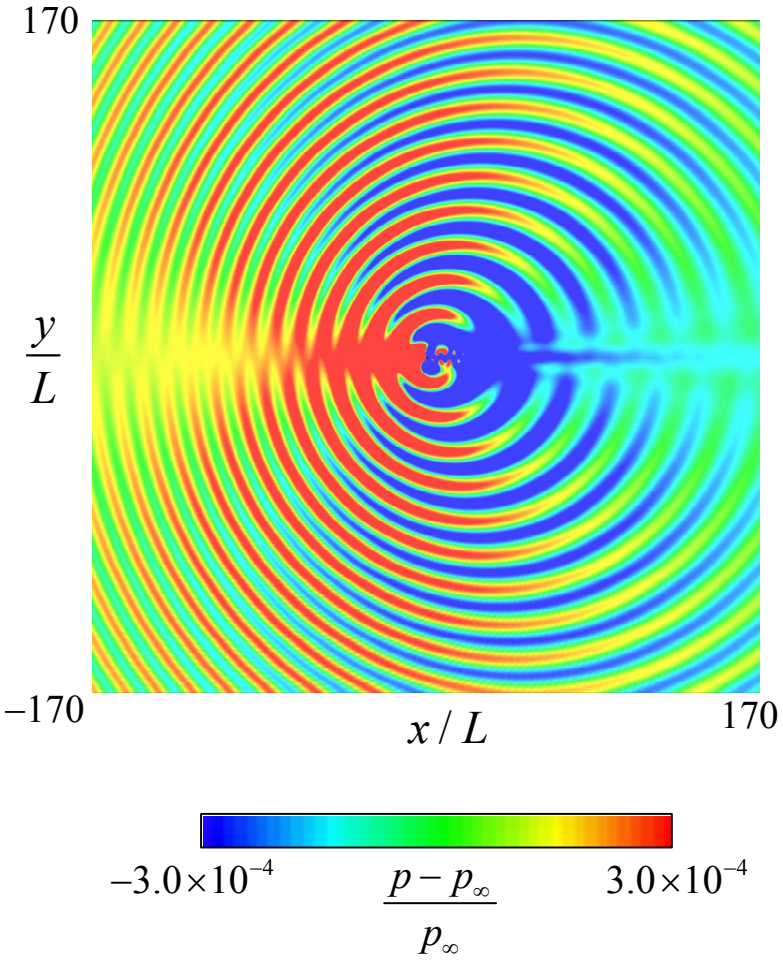

(a)

Figure 9 (continued to next page)

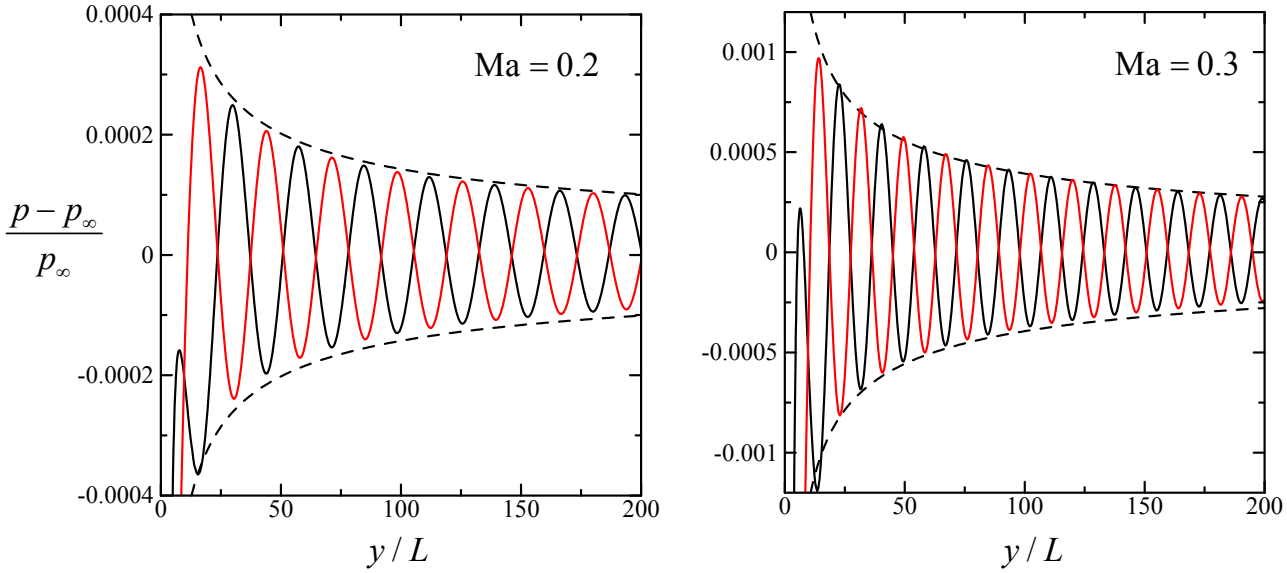

(b)

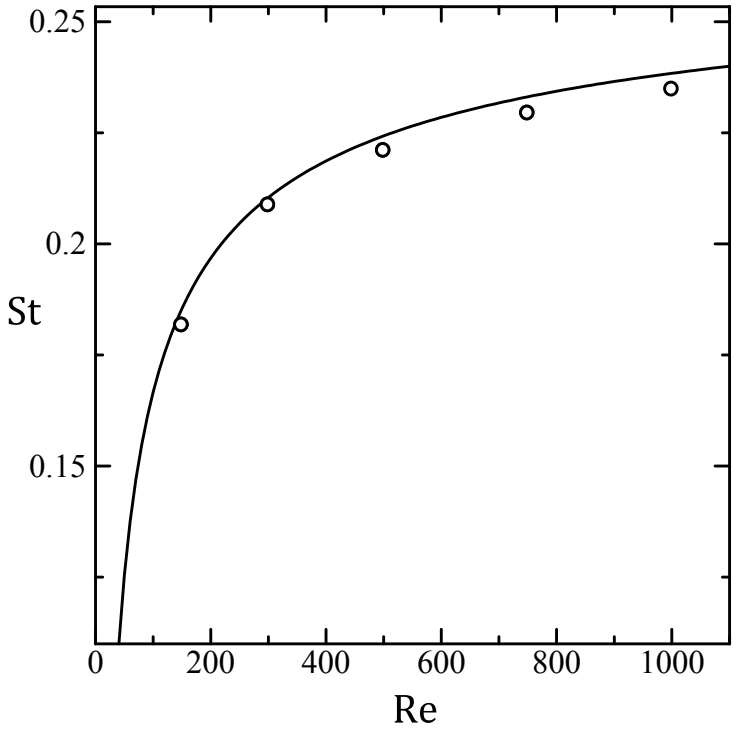

(c)

Figure 9

Table 1 Comparison of the pressure drag coefficient C_{dp}, friction drag coefficient C_{df}, total drag coefficient $C_{d\,\mathrm{total}}$, and total lift coefficient $C_{l\,\mathrm{total}}$ for a flow past NACA0012 airfoil.

References	C_{dp}	C_{df}	$C_{d\,\mathrm{total}}$	$C_{l\,\mathrm{total}}$
The present model	0.15097	0.12384	0.27481	0.45552
Jawahar & Kamath [32]	0.15287	0.12439	0.27726	0.50231
GAMM [33]	—	—	0.243-0.2868	0.4145-0.517
Yang et al. [34]	0.15353	0.13012	0.28365	0.43593